Energy, Environmental, and Catalysis Applications

Guidelines for all-solid-state battery design and electrode buffer layers based on chemical potential profile calculation

Takashi Nakamura, Koji Amezawa, Joern Kulisch, Wolfgang G. Zeier, and Jürgen Janek

ACS Appl. Mater. Interfaces, **Just Accepted Manuscript** • DOI: 10.1021/acsami.9b03053 • Publication Date (Web): 10 May 2019

Guidelines for all-solid-state battery design and electrode buffer layers based on chemical potential profile calculation

Takashi Nakamura[*1], *Koji Amezawa*[1], *Jörn Kulisch*[2], *Wolfgang G. Zeier*[3], *Jürgen Janek*[3]

[1] Institute of Multidisciplinary Research for Advanced Materials, Tohoku University, 2-1-1, Katahira, Aoba-ku, 980-8577 Sendai, Japan

[2] BASF SE, 67056 Ludwigshafen, Germany

[3] Institute of Physical Chemistry & Center for Materials Research, Justus-Liebig-University Giessen, Heinrich-Buff-Ring 17, 35392 Giessen, Germany

KEYWORDS: All-solid-state batteries, buffer layer, cathode coating, potential profile, potential distribution

ABSTRACT: Protective coatings on cathode active materials have become paramount for the implementation of solid-state batteries, however, the development of coatings lacks the understanding of the necessary coating properties. In this study, guidelines for the design of solid electrolytes and electrode coatings in all solid-state batteries are proposed from the viewpoint of the steady-state Li chemical potential profile across the battery cell. The model calculation of the (electro)chemical potential profile in all-solid-state batteries is established by considering the steady-state mixed ionic and electronic conduction in the solid electrolyte under the assumption of local equilibrium. For quantitative discussions, the potential profiles within oxygen ion conductors are calculated instead of Li/Na ion conductors as their partial electronic conductivities have not been reported so far in sufficient detail. Based on the calculated chemical potential profile, two main conclusions are obtained; (1) the decisive factor for the formation of the chemical potential profile of the neutral mobile component (e.g. oxygen or lithium) in the solid electrolyte is its electronic conductivity (and the activity dependence), and (2) a particularly large potential drop is formed in a region where the electronic conductivity becomes small. While these conclusions are valid and general for any solid electrolyte device, they are particularly important for the design of protective

coatings and the understanding of the functionality of self-assembled solid electrolyte interphases in all-solid-state batteries. To protect the solid electrolyte from decomposition by reduction/oxidation at the anode/cathode interfaces, a sufficient chemical potential drop is necessary within the coating layer or directly at the interphase layer. To achieve this situation, the coating/interphase materials need to have a lower electronic conductivity than the solid electrolyte.

1. Introduction

All-solid-state batteries (ASSBs) are promising candidates for next generation energy storage devices which are projected to be more efficient, safer and may achieve higher energy density than conventional lithium ion batteries (LIB)[1,2]. Towards the realization of high performance ASSBs, various solid electrolytes (SEs) have been proposed and studied[2–10], and different types of solid state rechargeable batteries have been demonstrated with Li^+, Na^+, and F^- ions as mobile charge carriers[8–12]. Despite their favorable transport properties, the thermodynamic stability of the prominent Li^+ and Na^+ conductors is suggested to be poor according to first-principle calculations and

experiments[13–21]. When the SE is exposed to a huge chemical potential difference between the cathode and the anode to ensure a high cell voltage, oxidation and reduction reactions lead to deterioration and poor long-term performance of ASSBs. In the case of solid-state Li ion batteries, the anode side of the SE is exposed to a high Li chemical potential μ_{Li} (high Fermi level, *i.e.*, low electric potential φ) while the cathode side of the SE is exposed to a low Li chemical potential μ_{Li} (low Fermi level, high electric potential φ). The theoretical stability window of the best Li ion conductors, the lithium thiophosphates, seems to be quite narrow and the stability limits are mostly much lower/higher than the Li chemical potentials of typically used anode and cathode materials[13,14]. This means that the SE in contact with anode/cathode active materials will decompose by reduction/oxidation even under open circuit conditions. Because such reduction/oxidation decomposition needs the transport of ions and electrons across the SEI, decomposition may be hindered apparently by very slow kinetics of ions and electron transport in SEs and SEIs. For the proper operation of ASSBs, a stable solid electrolyte interphase (SEI) needs to be formed at the interface to protect the SE from the decomposition either kinetically or thermodynamically, similar to the SEI formation in conventional LIBs using organic liquid electrolytes[22–24]. The formation

and the growth of the occurring interphases at the SE/anode interface and the SE/cathode interface were recently studied by in-situ X-ray photoemission spectroscopy, transmission electron microscopy, and electrochemical measurements[16–21]. While the growing interphase that is observed may protect a SE from a harsh chemical environment, the diffusion-controlled growth of the interphase results in the increase of the cell resistance and lead to capacity fading in ASSBs[18–21]. Protective coatings or self-assembled SEIs can be a solution to prevent the decomposition of the SE and undesirable side-reactions at the interface[16–21,25,26]. The chemical potential gap between the anode and the cathode is connected through a SEI/SE/coating multi-layer sequence by forming a potential slope through the cell as suggested by Mo and coworkers[14]. It is necessary to form a sufficient potential drop in the interphase and the coating layers in order to protect the solid electrolyte from decomposition. Otherwise, the chemical potential of lithium at the interface exceeds the stability limit of the SE and further decomposition of the SE will proceed. While this problem has been well described qualitatively already and counter measures have been intuitively proposed[13–15,27], we believe that a quantitative understanding of the potential profile in ASSBs is missing.

In this work, we describe a theoretical potential profile model for solid-state electrolyte devices based on solid-state thermodynamics and phenomenological transport theory. Although the goal of this work is the theoretical calculation of the steady-state potential profile through an ASSB cell, this cannot be accomplished due to the lack of partial conductivity data of Li^+/Na^+ conductors, especially the partial electronic conductivity as a function of Li/Na activity. In order to be able to discuss quantitative characteristics of the potential profile in SE devices regardless of this deficit, we first calculate the oxygen chemical potential profile in two different solid oxygen ion-conducting electrolytes, namely, yttrium-stabilized zirconia (YSZ) and gadolinia-doped ceria (GDC) as an example. Using the description derived from the oxygen ion conductors, we provide qualitative guidelines for the design of ASSBs based on the potential profile calculation. This work provides a descriptor for the properties of coating layers at electrode interfaces in order to minimize electrolyte decomposition in solid-state electrochemical devices.

2. Potential profile model for solid electrolyte devices

The major aim of this paper is to present a realistic phenomenological model for the lithium chemical potential profile in an ASSB cell based on solid-state thermodynamics and transport theory. The chemical potential profile in SEs was firstly demonstrated in the 1970's[28,29], and until now, successfully explains the chemical potential profiles and related transport phenomena in a wide variety of SE devices[30–34]. It is worth noting that (1) this phenomenological model is applicable to any SE device and (2) it relies on the consideration of both ionic and electronic transport in the SE. While the concentration of electronic charge carriers (both electrons and holes) in SE is small and their influence on the operation of SE devices is also small, the contribution of electronic conduction to the profile of the chemical potential of the neutral component along the electrochemical cell is essential. Just after cell fabrication, the potential profile is considered to be controlled by the formation of the electric potential φ near the electrode/SE interface, since the transport of electrons across the SE is very slow. This situation is similar to the electrostatic polarization of dielectric materials, and far from the steady-state. After some time, the electric potential along the SE will gradually change by the coupled diffusion of ions and electrons and finally the potential profile and the coupled ion/electron flux will reach the steady-state. In this case, considering

only the space charge effect (the screening effect of charge carriers) is not suitable to understand the potential profile in a SE device. Especially in high temperature SE devices, it is widely accepted that the dipole (electric double layer) at the electrode/electrolyte interface is negligibly small even under current load and that the applied external electric potential difference induces a change in the chemical potential of the neutral mobile component (e.g. oxygen or lithium)[35–38]. A wide electric potential distribution in the range of μm was observed at the cathode/SE interface of ASSBs by electron holography and Kelvin probe force microscopy[39,40]. The observed electric potential distribution is several orders of magnitude wider than the electric potential distribution estimated from the ionic carrier concentration and the electric permeability of SEs[41,42]. Even if an extreme carrier concentration change at the SE/electrode interface is assumed, it is still difficult to explain such a wide electric potential distribution with a space charge layer only. When coupled ion/electron diffusion is considered, on the other hand, a much wider potential distribution than that due to the screening effect is expected as earlier works suggested[30–34]. The contribution of coupled ion/electron diffusion is likely a more reasonable explanation for a very wide potential distribution at the SE/active material interface than so far reported screening

effects. As we will demonstrate in this work, a small electronic conductivity (σ_{el}) in the SE will lead to interesting and realistic conclusions concerning the chemical potential profile, and in particular on the role of electrode coatings and interphases.

Figure 1 shows schematic pictures of a SE cell exposed to a large chemical potential difference $\Delta\mu_A = \mu_A(L) - \mu_A(0)$, assuming operating conditions of batteries and fuel cells. The general component A may be any mobile (neutral) combination of an ion and electrons, e.g. oxygen (O), lithium (Li) or sodium (Na). In Fig. 1-a, a one-dimensional model of a single-layer system (anode / solid electrolyte / cathode) is considered. For the sake of simplicity, interface resistances and resulting electrode overpotentials are not included. In the steady-state, the divergence of ionic and electronic fluxes through the SE can be assumed to be zero, *i.e.*, $\nabla i_{el} = \nabla i_{ion} = 0$, with i_{el} and i_{ion} denoting the partial electronic and ionic current densities. This means that the partial currents of ions and electrons are constant and independent from the position in the SE. In the case that no net electric current is flowing, the open-circuit voltage (OCV) condition is maintained and the transport is only due to coupled chemical diffusion (ambipolar diffusion of ions and electron) across the SE. This

"paired" diffusion of ions and electrons is an important phenomenon in chemically inhomogeneous SEs, in which the "chemical inhomogeneity" is related to very small variation of the nonstoichiometry along the SE. Partial current densities of ions, i_{ion}, and that of electrons, i_{el}, depend linearly on the electrochemical potential gradients as driving forces:

$$i_{\mathrm{ion}} = -\frac{\sigma_{\mathrm{ion}}}{zF}\frac{\mathrm{d}\tilde{\mu}_{\mathrm{ion}}}{\mathrm{d}x} \quad (1)$$

$$i_{\mathrm{el}} = \frac{\sigma_{\mathrm{el}}}{F}\frac{\mathrm{d}\tilde{\mu}_{\mathrm{el}}}{\mathrm{d}x} \quad (2)$$

where z, F, σ_{ion}, σ_{el}, $\tilde{\mu}_{\mathrm{ion}}$ and $\tilde{\mu}_{\mathrm{el}}$ are the charge number of the mobile ion, the Faraday constant, the partial conductivity of the ions, that of electrons, the electrochemical potential of ions, and that of electrons, respectively (z = +1 for Li^+ and Na^+ and z = -2 for O^{2-}). Local equilibrium in the system is described by

$$\mu_{\mathrm{A}} = \tilde{\mu}_{\mathrm{ion}} + \mathrm{z}\tilde{\mu}_{\mathrm{el}} \quad (3\text{-}1)$$

$$\frac{\mathrm{d}\mu_{\mathrm{A}}}{\mathrm{d}x} = \frac{\mathrm{d}\tilde{\mu}_{\mathrm{ion}}}{\mathrm{d}x} + z\frac{\mathrm{d}\tilde{\mu}_{\mathrm{el}}}{\mathrm{d}x} \quad (3\text{-}2)$$

where μ_{A} is the chemical potential of the neutral chemical component corresponding to the carrier ion A^z (with A = Li, Na and O for Li^+, Na^+ and O^{2-}), respectively. To define the operating condition, the current ratio r is introduced as an important parameter.

$$r = {i_{\mathrm{ion}}}/{i_{\mathrm{el}}} \tag{4}$$

Here, $r > 0$, $r < -1$ and $r = -1$ represent the charge (or electrolysis), the discharge (spontaneous reaction in closed circuit) and open circuit conditions, respectively. When $r = -1$, internal ionic and electronic currents through the SE are balanced ($i_{\mathrm{ion}} + i_{\mathrm{el}} = 0$) and the net external current becomes zero, i.e. the open circuit condition has been reached. As can be confirmed by Eq. 4, the steady-state coupled diffusion of ions and electrons always exists in the SE, even under open circuit condition. Using Eqs. 1-4, the gradient of the electrochemical potential of both ions and electrons can be described by the slope of the chemical potential of the neutral component.

$$\frac{\mathrm{d}\tilde{\mu}_{\mathrm{ion}}}{\mathrm{d}x} = -\frac{r\sigma_{\mathrm{el}}}{\sigma_{\mathrm{ion}} - r\sigma_{\mathrm{el}}}\frac{\mathrm{d}\mu_{\mathrm{A}}}{\mathrm{d}x} \tag{5-1}$$

$$\frac{\mathrm{d}\tilde{\mu}_{\mathrm{el}}}{\mathrm{d}x} = \frac{1}{\mathrm{z}}\frac{\sigma_{\mathrm{ion}}}{\sigma_{\mathrm{ion}} - r\sigma_{\mathrm{el}}}\frac{\mathrm{d}\mu_{\mathrm{A}}}{\mathrm{d}x} \tag{5-2}$$

The relationships between partial current densities and chemical potential are obtained from Eqs. 1, 2 and 5.

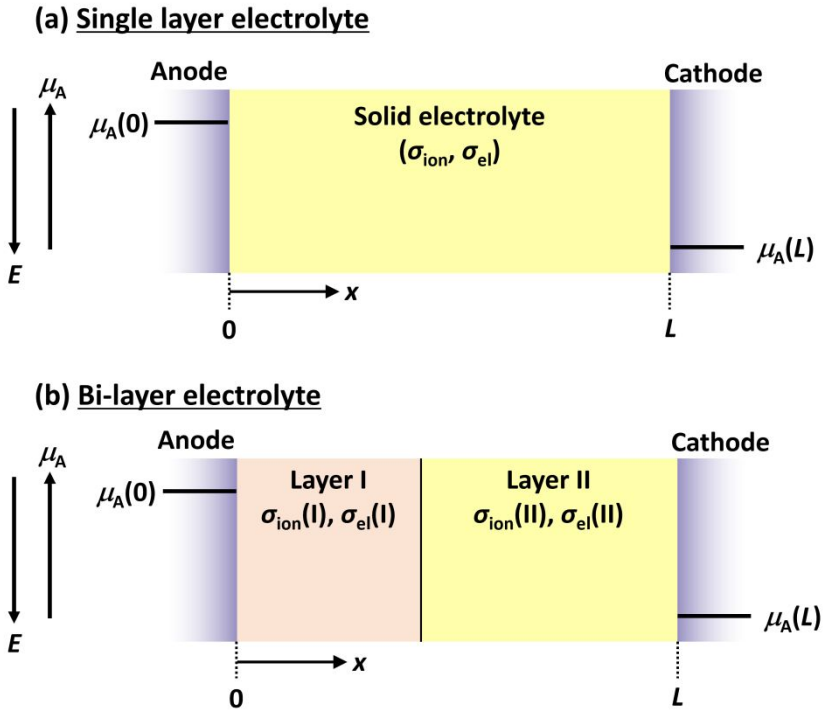

Figure 1. Schematic illustrations of solid electrolyte systems. (a) Single layer electrolyte and (b) bi-layer electrolyte simulating SE/coating and SEI/SE systems. μ_A represents the neutral chemical potential of A of a mobile cation A^z in the SE.

$$i_{\text{ion}} = \frac{r}{zF}\frac{\sigma_{\text{ion}}\,\sigma_{\text{el}}}{\sigma_{\text{ion}} - r\sigma_{\text{el}}}\frac{d\mu_A}{dx} \qquad (6\text{-}1)$$

$$i_{\mathrm{el}} = \frac{1}{\mathrm{z}F}\frac{\sigma_{\mathrm{ion}}\,\sigma_{\mathrm{el}}}{\sigma_{\mathrm{ion}} - r\sigma_{\mathrm{el}}}\frac{\mathrm{d}\mu_{\mathrm{A}}}{\mathrm{d}x} \qquad (6\text{-}2)$$

Then, we assume zero divergence of ionic and electronic partial currents in the SE in the steady-state, meaning there is no sink and source for ions and electron in the SE. This assumption is realistic when μ_{A} lies within the stable potential window of the SE and the nonstoichiometric variation in the SE is negligibly small. Due to these assumptions, constant partial currents are obtained at any position in the SE in the steady-state. By considering the continuity equation for partial current densities, $i_{\mathrm{j}}(x_2 - x_1) = \int_{x_1}^{x_2} i_{\mathrm{j}}\mathrm{d}x$ (j = ion or electron), one can obtain the potential profile, μ_{A} vs. *x*/*L*, in a single layer SE system for a given operating condition described by the parameter *r*.

$$\frac{x}{L} = \frac{\int_{\mu_{\mathrm{A}}(0)}^{\mu_{\mathrm{A}}(x)} \frac{\sigma_{\mathrm{ion}}\,\sigma_{\mathrm{el}}}{\sigma_{\mathrm{ion}} - r\sigma_{\mathrm{el}}}\mathrm{d}\mu_{\mathrm{A}}}{\int_{\mu_{\mathrm{A}}(0)}^{\mu_{\mathrm{A}}(L)} \frac{\sigma_{\mathrm{ion}}\,\sigma_{\mathrm{el}}}{\sigma_{\mathrm{ion}} - r\sigma_{\mathrm{el}}}\mathrm{d}\mu_{\mathrm{A}}} \qquad (7)$$

where $\mu_{\mathrm{A}}(x)$ is the chemical potential at the position *x*. From the relation of $-FE = \Delta\tilde{\mu}_{\mathrm{el}}$, the distribution of the electric potential in the SE can be calculated by

$$E = \frac{1}{F}\int_{\mu_A(0)}^{\mu_A(x)} \frac{\sigma_{ion}}{\sigma_{ion} - r\sigma_{el}} d\mu_A \quad (8)$$

While the assumption of a single layer electrolyte configuration may be the case in some solid-state batteries during assembly, the reactions of the lithium metal anode as well as the cathode with the SE make protective coatings and SEIs necessary. Therefore, to consider the potential profile in the coating and the interphases layers as well as the SE layer, a bi-layer electrolyte configuration is needed (Figure 1-b). Assuming that the (electro)chemical potentials are constant in the anode and the cathode active material, and since the condition of constant partial currents in the steady-state is also applicable to bi-layer SE systems, Eqs. 7 and 8 can be applied to a bi-layer SE system by separating the integration range.

(i) μ_A and E profiles in the layer I ($0 < x < x_{int}$)

$$\frac{x}{L} = \frac{\int_{\mu_A(0)}^{\mu_A(x)} \frac{\sigma_{ion}(I)\,\sigma_{el}(I)}{\sigma_{ion}(I) - r\sigma_{el}(I)} d\mu_A}{\int_{\mu_A(0)}^{\mu_A(x_{int})} \frac{\sigma_{ion}(I)\,\sigma_{el}(I)}{\sigma_{ion}(I) - r\sigma_{el}(I)} d\mu_A + \int_{\mu_A(x_{int})}^{\mu_A(L)} \frac{\sigma_{ion}(II)\,\sigma_{el}(II)}{\sigma_{ion}(II) - r\sigma_{el}(II)} d\mu_A} \quad (9\text{-}1)$$

$$E = \frac{1}{F}\int_{\mu_A(0)}^{\mu_A(x)} \frac{\sigma_{ion}(I)\,\sigma_{el}(I)}{\sigma_{ion}(I) - r\sigma_{el}(I)} d\mu_A \quad (9\text{-}2)$$

(ii) μ_A and E profiles in the layer II ($x_{int} < x < L$)

$$\frac{x}{L} = \frac{\int_{\mu_A(0)}^{\mu_A(x_{int})} \frac{\sigma_{ion}(I)\,\sigma_{el}(I)}{\sigma_{ion}(I) - r\sigma_{el}(I)} d\mu_A + \int_{\mu_A(x_{int})}^{\mu_A(x)} \frac{\sigma_{ion}(II)\,\sigma_{el}(II)}{\sigma_{ion}(II) - r\sigma_{el}(II)} d\mu_A}{\int_{\mu_A(0)}^{\mu_A(x_{int})} \frac{\sigma_{ion}(I)\,\sigma_{el}(I)}{\sigma_{ion}(I) - r\sigma_{el}(I)} d\mu_A + \int_{\mu_A(x_{int})}^{\mu_A(L)} \frac{\sigma_{ion}(II)\,\sigma_{el}(II)}{\sigma_{ion}(II) - r\sigma_{el}(II)} d\mu_A} \quad (9\text{-}3)$$

$$E = \frac{1}{F}\left(\int_{\mu_A(0)}^{\mu_{A(x_{int})}} \frac{\sigma_{ion}(I)}{\sigma_{ion}(I) - r\sigma_{el}(I)} d\mu_A + \int_{\mu_{A(x_{int})}}^{\mu_A(x)} \frac{\sigma_{ion}(II)}{\sigma_{ion}(II) - r\sigma_{el}(II)} d\mu_A \right) \quad (9\text{-}4)$$

3. Results and discussion

3.1. Potential profile in solid electrolyte systems (example of oxygen ion conductors)

The potential profile model we propose here has been applied to many different SE devices using O^{2-}, H^+, Ag^+ conductors, and successfully explained the potential distribution in the corresponding solid electrolytes[30–34]. Due to the underlying transport phenomena of all these ion conductors, the model is considered to be applicable to any SE device. Therefore, the steady-state potential model also provides important knowledge about the chemical potential profile in an ASSB cell. As discussed in Section 2, the parameters, σ_{ion}, σ_{el}, $\mu_A(0)$, $\mu_A(L)$, T, and r are needed for the potential profile calculation. In addition, the activity dependence of the partial conductivities ($\sigma_{ion}(a(A))$ and $\sigma_{el}(a(A))$) are required for the qualitative potential profile calculation,

because the local electronic concentration varies with the nonstoichiometry. The ionic conductivity σ_{ion} of most SEs is constant throughout a cell as it is an intrinsic parameter due to structural disorder, or due to the high concentration of ionic carriers. On the other hand, σ_{el} of the SE significantly depends on the chemical state of the SE, in other words, σ_{el} depends on the local chemical potential μ_A. Unfortunately, no sufficient electronic conductivity data of recently developed Li^+ and Na^+ conductors have been reported so far, especially the Li or Na activity dependence of σ_{el} is virtually unknown. In order to circumvent the lack of data in the literature, we apply typical oxygen ion conductors, $(Y_2O_3)_{0.08}(ZrO_2)_{0.92}$ (YSZ) and $Ce_{0.9}Gd_{0.1}O_{1.95}$ (GDC) as model SE. Here, the potential profile within a given chemical potential difference $\Delta\mu_O$ was calculated quantitatively instead of the chemical potential μ_{Li} (μ_{Na}) of Li^+ and Na^+ conductors, because the partial conductivities of YSZ and GDC have been studied. In particular, the partial electronic conductivity in YSZ is order of magnitude lower than the ionic conductivity, whereas the partial electronic conductivity in GDC is high and similar to the ionic conductivity. These particular examples provide a good description of the chemical potential profile across a solid-state device depending on the ratio of electronic and ionic partial conductivities. In fact, GDC represents a SE that is easily

reduced at the low μ_O side, and that can be protected by YSZ. The calculated chemical potential profile provides us with a better understanding about how chemical and electric potentials distribute across the SE, irrespective of the specific ionic charge carrier.

Before calculating the potential profile, some important considerations about the SE are summarized below. Figure 2 shows the partial conductivities of YSZ and GDC from literature data[43,44]. Since these oxides show a high concentration of oxygen vacancies as an ionic charge carrier due to massive acceptor doing, the oxygen ion conductivity, $\sigma_{O^{2-}}$, is invariant regardless of the oxygen chemical potential which is expressed as log $p(O_2)$ in the figure (log $p(O_2) = (\mu(O_2)-\mu^\circ(O_2))/RT$). Here, σ_{el}, a sum of electron conductivity (σ_n) and hole conductivity (σ_p), strongly depends on the oxygen chemical potential. This is caused by the change of the electron/hole concentration due to the oxygen vacancy formation/annihilation.

Hole formation at high $p(O_2)$: $V_O^{\cdot\cdot} + \frac{1}{2}O_2 \rightarrow O_O^{\times} + 2h^{\cdot}$ (10-1)

Electron formation at low $p(O_2)$: $O_O^{\times} \rightarrow V_O^{\cdot\cdot} + \frac{1}{2}O_2 + 2e'$. (10-2)

The oxygen vacancy concentration changes due to the defect formation (Eq. 10) are much smaller than the oxygen vacancy concentration formed by the initial acceptor doping. Therefore, $\sigma_{O^{2-}}$ can be considered as constant regardless of the oxygen chemical potential. In terms of the electronic partial conductivity, the intrinsic electronic carrier concentration is small in both YSZ and GDC due to the wide band gap of the materials. Thus, the concentration of electrons and holes changes strongly with changing extrinsic defect formation (Eq. 10). Considering the defect formation mechanism shown in Eq. 10, the concentration of electrons is proportional to $p(O_2)^{-1/4}$ and that of holes is proportional to $p(O_2)^{1/4}$. Therefore, σ_{el} of oxygen ion conductors can generally be expressed as follows,

$$\sigma_{el} = \sigma_h^o p(O_2)^{1/4} + \sigma_e^o p(O_2)^{-1/4} \quad (11)$$

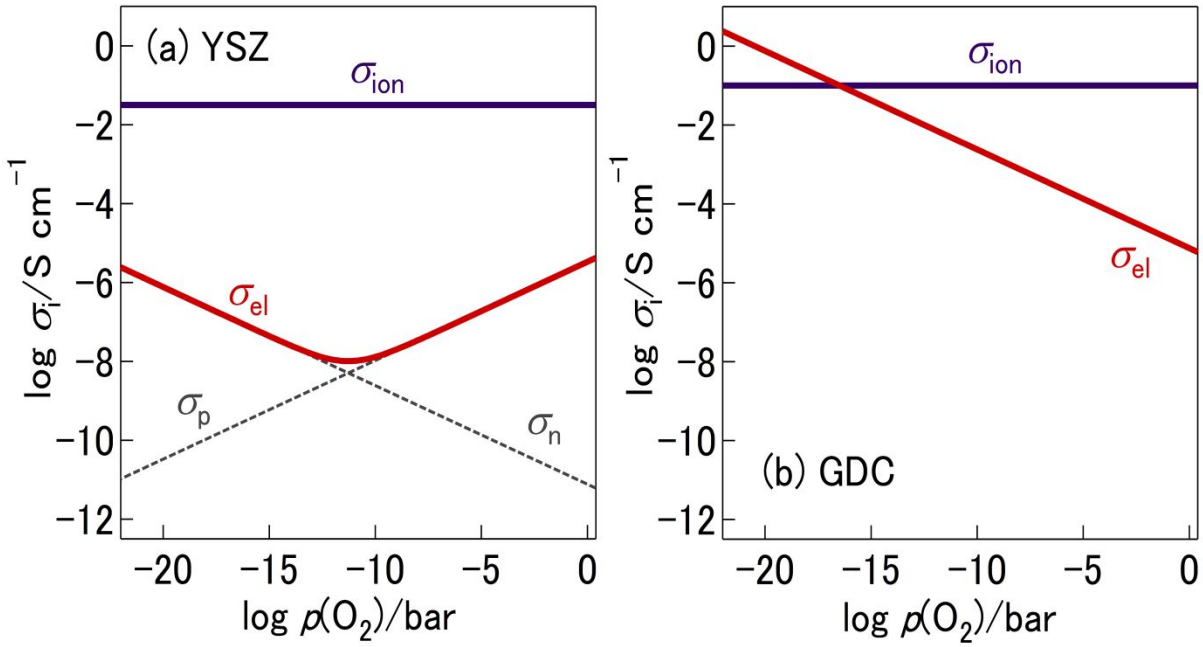

Figure 2. $p(O_2)$ dependence of partial electronic conductivities of (a) $(Y_2O_3)_{0.08}(ZrO_2)_{0.92}$ and (b) $Ce_{0.9}Gd_{0.1}O_{1.95}$ at 1073 K[43,44]. Reproduced with permission from references 43 and 44. Copyright 1989 and 2000 Electrochemical Society.

where σ_h^0 and σ_e^0 are the hole conductivity and the electronic conductivity under 1 bar O_2 atmosphere, respectively. The concentration of electrons at log $p(O_2)$ = -20 is 10^5 times higher than that at log $p(O_2)$ = 0, while the concentration of holes at log $p(O_2)$ = 0 is 10^5 times higher than that at log $p(O_2)$ = -20. As shown in Figure 2, these concentration changes lead to a significant variation of σ_{el}. Reported partial conductivities ($\sigma_{O^{2-}}$, σ_h^0 and σ_e^0) of YSZ and GDC are summarized in Table 1[43,44]. The

variation of the electronic conductivity due to defect formation as a function of the chemical potential of the neutral component (O in the case of oxygen SE) is important and a general property of SEs. In ASSB cells, the SE facing the anode and the cathode active materials will reach local equilibrium and the SE at the cathode side and at the anode side will show quite different transport properties. Both sides have almost the same concentration of ionic charge carriers and very different concentrations of electronic carriers, (by orders of magnitude). This does not affect the actual battery (or fuel cell) performance – which depends primarily on the ionic conductivity of the SE, but has a strong influence on the chemical potential profile in the ASSB cell. Similar to other SE systems, the local σ_{el} of Li^+ conductors and that of Na^+ conductors also depend on the μ_{Li} and μ_{Na} distribution fixed at the ends of the SE by local equilibrium with the active materials. For Li ion conductors, we can consider the variation of partial electronic conductivities due to Li defect formation/annihilation in the similar manner. Defect equilibria and schematic Brouwer

diagrams of Li ion conductors are summarized by Maier[45].

Table 1. Partial conductivities of $(Y_2O_3)_{0.08}(ZrO_2)_{0.92}$ and $Ce_{0.9}Gd_{0.1}O_{1.95}$ at 1073 K[43,44].

	$\sigma_{O^{2-}}$/S cm^{-1}	σ_h^o/S cm^{-1}	σ_e^o/S cm^{-1}
$(Y_2O_3)_{0.08}(ZrO_2)_{0.92}$ [43]	0.032	3.3×10^{-6}	7.7×10^{-12}
$Ce_{0.9}Gd_{0.1}O_{1.95}$ [44]	0.1	-	7.6×10^{-6}

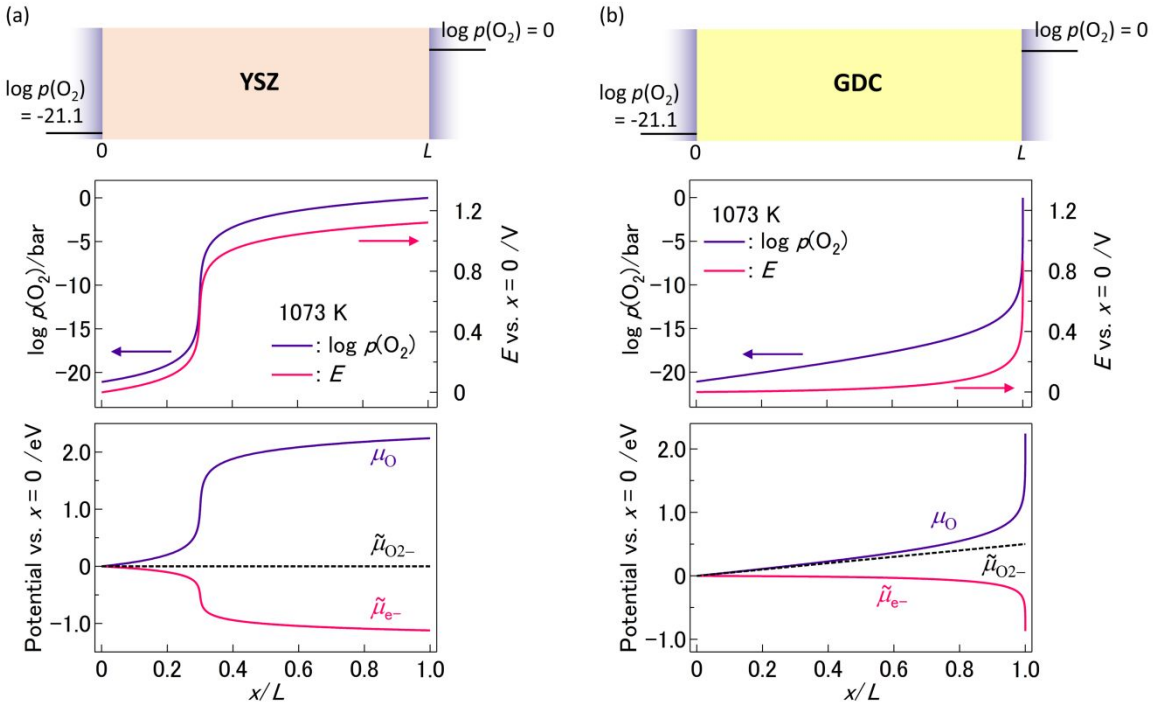

Figure 3. Potential profile in (a) YSZ and (b) GDC within an externally controlled μ_O difference; T = 1073 K, r = -1 (open circuit), log $p(O_2)$ = 0 at x = 0 (corresponds to 1 bar O_2) and log $p(O_2)$ = -21.1 at x = L (corresponds to 4.2% humidified H_2).

The potential profiles in YSZ and GDC within a given oxygen chemical potential difference were calculated assuming the "fuel cell open circuit condition"; T = 1073 K, r = -1 (open circuit), log $p(O_2)$ = 0 at x = 0 (corresponds to 1 bar O_2) and log $p(O_2)$ = -21.1 at x = L (corresponds to 4.2% humidified H_2). Except the high temperature condition, the situation of the SE is equivalent to ASSBs. One side of the SE is exposed to a high chemical potential condition and the opposite side is exposed to the low chemical potential condition. This chemical potential difference between the anode

and the cathode is taken up by the SE layer. To highlight one important characteristics of the potential profile within the SE, we calculate the effective local oxygen partial pressure from μ_O as follows:

$$\mu_O = \mu_O^\circ + \frac{RT}{2}\ln\left(\gamma_O p(O_2)/p^\circ(O_2)\right) \quad (12)$$

where μ_O°, T, γ_O and $p^\circ(O_2)$ are the standard oxygen chemical potential, the temperature, the activity coefficient for oxygen and the standard oxygen pressure (1 bar), respectively. In the calculation, γ_O = 1 is assumed. Figure 3 shows the potential profile (the distribution of log $p(O_2)$, E, μ_O, $\tilde{\mu}_{el}$ and $\tilde{\mu}_{O^{2-}}$) in YSZ and GDC, in which the oxygen chemical potential profile in YSZ is totally different from that in GDC. These results clearly show the impact of electronic defect equilibria in the SE on the potential profile. In other words, depending on the partial electronic conductivities and their dependence on the chemical potential, the chemical potential profile and drop across the SE will be quite different. As described above, steady-state coupled diffusion of O^{2-} and electrons, so-called ambipolar diffusion, proceeds under the open circuit condition. The local potential gradient drives the motion of the minor carriers, electrons and holes, together with oxygen ions, which leads to permeation of the neutral

component oxygen (O) across the SE. In solid oxide fuel cells, this minor permeation flux of oxygen does not play an important role, while the permeation flux of hydrogen through proton-conducting ceramics fuel cells significantly lowers the efficiency of the energy conversion of fuels to electricity[34]. In solid-state lithium ion batteries, this permeation flux of Li may be critical, as it defines the self-discharge rate of a charged battery – i.e. a very small electronic partial conductivity is desired to keep the self-discharge rate low.

To maintain zero net current ($i_{ion} + i_{el} = 0$), a negligibly small driving force $\frac{d\tilde{\mu}_{ion}}{dx}$ acts on the ions, and a large driving force $\frac{d\tilde{\mu}_{el}}{dx}$ will be formed in the SE, as σ_{ion} is much larger than σ_{el}. σ_{el} changes locally depending on the effective oxygen chemical potential in line with the defect formation equilibria (Eq. 10). As shown in Figure 2, a small σ_{el} is obtained at high $p(O_2)$ for GDC, and at around log $p(O_2)$ = -12 for YSZ. Because the steepest potential gradient is formed where σ_{el} is the smallest, the steepest gradients $\frac{d\tilde{\mu}_{el}}{dx}$ and $\frac{d\mu_O}{dx}$ are formed at the high $p(O_2)$ boundary ($x = L$) for GDC, and at the middle of the SE where log $p(O_2)$ is close to -12 for YSZ. Therefore, the most influential factor for the steady-state potential profile in SEs is indeed the

electronic conductivity (and its activity dependence). The tendency of the potential profile to form a large potential drop where σ_{el} has its minimum, is also valid for a bi-layer electrolyte system which simulates the potential profile through the sequence of an active material AM with AM-I/SEI/SE/AM-II and AM-I/coating/SE/AM-II. As shown in Figure 1-b, we assume a constant (electro)chemical potential in the cathode and anode active materials. One layer of the bi-layer electrolyte represents the SE and the other layer represents the coating or the SEI. As a demonstration, the potential profiles in two different bi-layer electrolyte systems, (a) L(YSZ)/L(GDC) = 1:9 with L(YSZ) = x_{int} and L(GDC) = L - x_{int} and (b) L(GDC)/L(YSZ) = 1:9 with L(GDC) = x_{int} and L(YSZ) = L - x_{int}, under open circuit, charging and discharging conditions were calculated and shown in Figure 4. In the Figure (a), the thinner layer (YSZ) simulates the cathode coating or SEI and the thicker layer (GDC) simulates the SE. Although 10% of the total electrolyte thickness is too thick for coatings or SEIs in ASSBs, we choose thick bi-layer structure to clearly visualize the potential profile in bi-layer electrolyte systems. Using the potential profile calculations, one can confirm that a similar potential profile is obtained also in thin layer systems. It is worth noting that similar bi-layer SE were studied as a functional electrolyte for solid oxide fuel cells. Bi-layer SOFC electrolytes

is summarized in ref. 46[46]. For instance, the YSZ layer at low $p(O_2)$ side can suppress the electronic conduction and the permeation of oxygen through a ceria-based electrolyte[46,47], and YSZ or ceria layers at the lower $p(O_2)$ side hinder decomposition of Bi_2O_3-based electrolytes by reduction[48–50]. In the YSZ/GDC bi-layer electrolyte, very thin protective layer (1/10000 to 1/1000 of the total thickness) successfully decrease undesired electronic conductivity while keeping high ionic

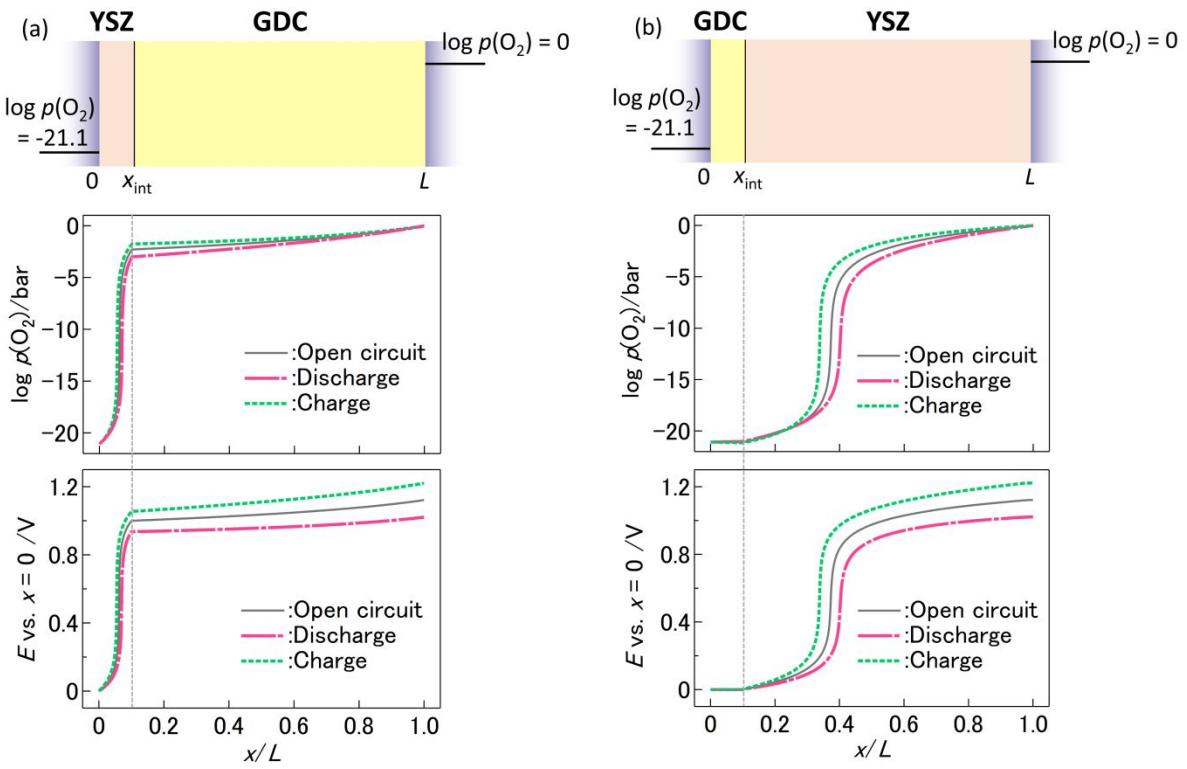

Figure 4. Potential profile in a bi-layer electrolyte under open circuit, 100 mV charge and 100 mV discharge conditions. (a) L(YSZ)/L(GDC) = 1:9 with L(YSZ) = x_{int} and L(GDC) = L - x_{int} and (b) L(GDC)/L(YSZ) = 1:9 with L(GDC) = x_{int} and L(YSZ) = L - x_{in} in a μ_O difference; T = 1073 K, log $p(O_2)$ at x = 0 is 0 (corresponds to 1 bar O_2) and log $p(O_2)$ at x = L is -21.1 (corresponds to 4.2% humidified H_2).

conductivity, which was proved experimentally and theoretically[46]. As shown in the graph, a huge chemical potential drop is formed in the YSZ layer (low σ_{el} layer) and a moderate potential drop is formed in the GDC layer (high σ_{el} layer), regardless of the length ratio of the bi-layer. Especially in the case of Figure 4-b, a small chemical potential difference builds up in the GDC layer. The potential profile is essentially determined by the coupled diffusion of ions and electrons. Therefore, to keep a steady-state

coupled ion/electron flux, the biggest driving force (= the steepest slope of electrochemical potential of electron) is necessary at the layer at which the electronic conductivity is the lowest. In the bi-layer system, the steeper potential drop is formed in the layer with the lower σ_{el}. Under current load, the potential profile in the SE changes slightly from that under the open circuit condition. In Figure 4, the potential profiles under 100 mV ohmic loss during charging (green dashed-line) and discharging (pink dashed-dotted line) are shown as a charging state and a discharging state, respectively. For the comparison, μ_O at x = 0 and L were fixed as -21.1 and 0, respectively. While the effective chemical potential at the anode and the cathode in an actual ASSB cell change with the state of charge of the active materials and electrode overpotentials, the latter were not included for the sake of simplicity. Compared with the open circuit condition, the potential profile becomes slightly steeper during charging while it becomes slightly flatter during discharging. However, the general shape of the potential profile under current load is similar to that under the open circuit condition. Therefore, even under current load, it is important to consider the contribution of mobile electrons in the SE to the chemical potential profile formation.

3.2. Guidelines for the design of all-solid-state batteries

In this section, we derive quantitative guidelines for the design of an ASSB cell from the steady-state potential profile calculation. Figure 5 shows schematic pictures of the steady-state potential profile near the anode/SEI/SE and the SE/coating/cathode of an ASSB cell. For simplicity, the chemical potential profile is expressed by straight lines, although the linear distribution is not realistic as shown in Figures 3 and 4. To avoid reductive decomposition of the SE at the anode side, the Li chemical potential at the SEI/SE interface, $\mu_{\mathrm{Li}}(\mathrm{int,A})$, should be lower than the reduction limits of the SE, $\mu_{\mathrm{Li}}(\mathrm{SE,red})$, by forming a sufficient potential drop in the SEI layer. To protect the SE from reductive decomposition, the SEI layer needs to have a smaller σ_{el} than the SE. In this case (Figure 5-a), a sufficient potential drop is formed in the SEI layer. On the contrary, when σ_{el} of the SEI is higher than that of the SE, a sufficient

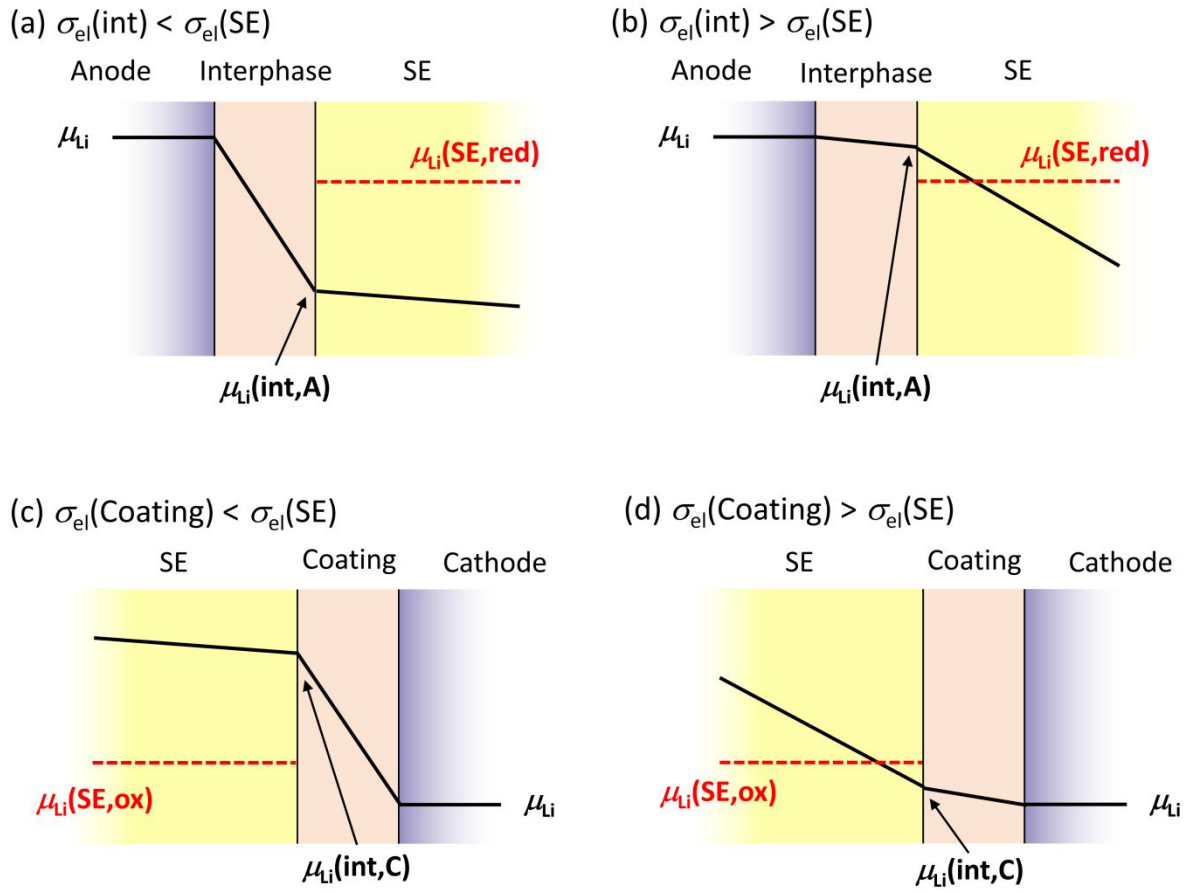

Figure 5. Schematic illustrations of the potential profile near the anode side (a and b) and near the cathode side (c and d). $\mu_{Li}(SE,red)$, $\mu_{Li}(SE,ox)$, $\mu_{Li}(int,A)$ and $\mu_{Li}(int,C)$ are the stability limit of reduction and oxidation of the solid electrolyte, the neutral Li chemical potential at the SEI/SE interface and that at the coating/SE interface.

potential drop cannot be expected in the SEI layer. In this case (Figure 5-b), the SEI layer will keep growing by decomposing the neighboring SE. This can be the cause of gradual increase of interfacial resistance or overpotential[18–20]. Detailed information on the potentials improves our understanding of the mechanism of interphase formation/growth and their functionalities. The same idea can be easily transferred to

the cathode coatings. To protect the SE from oxidative decomposition, the coating material must have a lower σ_{el} than the SE, to form a sufficient potential drop in the protective coating (Figure 5-c). When the Li chemical potential at the SE/coating interface, $\mu_{\mathrm{Li}}(\mathrm{int,C})$, is higher than the oxidation limit of the SE, $\mu_{\mathrm{Li}}(\mathrm{SE,ox})$, the coating successfully protects the SE from oxidative decomposition. When the coating material has a higher σ_{el} than the SE, no sufficient potential drop is formed in the coating. In this case, the SE will decompose by oxidation (Figure 5-d). While it is often proposed that high dielectric constant materials could mitigate the space charge and charge carrier depletion layers[51–53], our model suggests that the chemical potential profile is the reason why electronically insulating materials, wide band gap materials such $LiNbO_3$, are often chosen successfully as a cathode coating material[9,10,17]. To create a functional coating that protects the SE, one needs to select suitable coating materials and solid-electrolyte interphase layer that provide stability as well as good electrochemical performance. For instance, mixed Li^+ and e^- conductor coatings may be able to reduce the interfacial resistance if they can supply sufficient flux of ions and electrons to the surface of the active material. For mixed conductor coatings, however, only a small potential drop in the coating layer is expected, and hence the coating

does not mitigate the reductive/oxidative environment of the anode/cathode active materials. A more stable SE is required to exploit mixed conductor coatings. It is important to highlight that the functionality of the coating and the SEI layers, especially the formation of a potential drop, depend on the electronic conductivity of the SE as well as that of the coating and the SEI – the coating/SE combination needs to be optimized as a system. If the same low electronic conductivity material is used as coating with given thickness, the expected potential drop in the coating layer will increase with increasing electronic conductivity of the SE. Similarly, if a SE with extremely low electronic conductivity is used, it will be difficult to find a coating material with an even lower electronic conductivity that can form a sufficient potential drop in the coating layer. This might be a critical issue for the protection of polymer solid electrolytes that usually show an extremely small electronic partial conductivity.

As increasing the electronic conductivity of the SE will lead to a much faster self-discharge, the combination of a low electronic conductivity of the protection layer as well as of the SE are of paramount importance the long-term operation of an ASSB. For the design of the protective coating, one can calculate the optimum thickness of

the coating layer if the potential profile is understood quantitatively. For that, not only σ_{ion} but also the activity dependence of σ_{el} of the SE and the coating material are required. Partial conductivities can be evaluated by Hebb-Wagner measurement while the choice of suitable reversible electrodes for Li^+ and Na^+ conductors may be difficult due to the narrow thermodynamic potential window of SEs. Understanding partial conductivities of battery materials and the quantitative potential profile calculation are essential for further development of ASSBs.

Conclusion

In this study, the general characteristics of the chemical potential profile in a solid electrolyte separator or membrane is analyzed by considering mixed ionic and electronic conduction through the solid electrolyte. Comparing two model systems of electrolytes - one with similar electronic and ionic partial conductivity (a “true” MIEC) as well as one with orders of magnitude different partial conductivities (a “true” solid electrolyte) - shows how different the chemical potential profile develops at interfaces of two ionic conductors. Based on the calculated potential profiles, guidelines for the

design of all solid-state batteries are proposed. According to the results of the steady-state potential profile calculation, the following conclusions are obtained:

(1) A large potential drop is formed where the electronic conductivity is small, suggesting that the electronic conductivity of the solid electrolyte is the decisive factor for the chemical potential profile of lithium in all solid-state lithium batteries. As the calculation is quite general, this is of course true for sodium-based batteries.

(2) In order to protect the solid electrolyte from reductive/oxidative decomposition at the anode and the cathode, a sufficient potential drop is needed at the interface. This can only be achieved when the interphases and/or the coatings have a smaller electronic partial conductivity than the solid electrolyte itself.

Based on these findings, a coating material for solid-state batteries needs to be selected based on the following design concept. It needs to support a sufficient electrochemical performance as well as lead to a better interfacial stability. While mixed Li^+ and electron conductor coatings are likely effective to facilitate the electrochemical performance, only Li^+ conducting but electronically insulating coatings are effective to protect the solid electrolyte from oxidative/reductive decomposition.

While this statement as such appears trivial, our quantitative model leads to the stricter requirement that the partial electronic conductivity of the coating or the SEI needs to be lower than the partial electronic conductivity of the SE. As the partial electronic conductivities of SE are often not well know, this result also highlights the need for a better electrical characterization of SEs. We believe that our work provides a better quantitative understanding of protective coatings, helping with the future design of all-solid-state batteries.

ASSOCIATED CONTENT

Supporting Information

The supporting information contains an excel macro file for potential profile calculations (xlsm file) as well as the calculated results for the here shown potential profiles (xlsx file).

AUTHOR INFORMATION

Corresponding Authors

*Takashi Nakamura

Institute of Multidisciplinary Research for Advanced Materials, Tohoku University, 2-1-1, Katahira, Aoba-Ku, Sendai, 980-8577, Japan

Tel.: +81-22-217-5341

takashi.nakamura.e3@tohoku.ac.jp

Author Contributions

The manuscript was written through contributions of all authors. All authors have given approval to the final version of the manuscript.

Funding Sources

This work was supported by the International Network for Electrochemistry and Batteries of BASF SE, and the Research Program for CORE lab of "Dynamic Alliance for Open Innovation Bridging Human, Environment and Materials" in "Network Joint Research Center for Materials and Devices".

ACKNOWLEDGMENT

This work was supported by the International Network for Electrochemistry and Batteries of BASF SE, and the Research Program for CORE lab of "Dynamic Alliance for Open Innovation Bridging Human, Environment and Materials" in "Network Joint Research Center for Materials and Devices".

REFERENCES

(1) Janek, J.; Zeier, W. G. A Solid Future for Battery Development. *Nat. Energy* **2016**, *1*, 16141.

(2) Kim, J. G.; Son, B.; Mukherjee, S.; Schuppert, N.; Bates, A.; Kwon, O.; Choi, M. J.; Chung, H. Y.; Park, S. A Review of Lithium and Non-Lithium Based Solid State Batteries. *J. Power Sources* **2015**, *282*, 299–322.

(3) Goodenough, J. B.; Hong, H. Y.-P.; Kafalas, J. A. Fast Na^+ Ion Transport in Skelton Structures. *Mater. Res. Bull.* **1976**, *11*, 203–220.

(4) Hong, H. Y. P. Crystal Structure and Ionic Conductivity of $Li_{14}Zn(GeO_4)_4$ and Other New Li^+ Superionic Conductors. *Mater. Res. Bull.* **1978**, *13*, 117–124.

(5) Aono, H.; Imanaka, N.; Adachi, G. High Li^+ Conducting Ceramics. *Acc. Chem. Res.* **1994**, *27*, 265–270.

(6) Inaguma, Y.; Liquan, C.; Itoh, M.; Nakamura, T.; Uchida, T.; Ikuta, H.; Wakihara, M. High Ionic Conductivity in Lithium Lanthanum Titanate. *Solid State Commun.* **1993**, *86*, 689–693.

(7) Thangadurai, V.; Kaack, H.; Weppner, W. J. F. Novel Fast Lithium Ion Conduction in Garnet-Type $Li_5La_3M_2O_{12}$ (M = Nb, Ta). *J. Am. Ceram. Soc.* **2003**, *86*, 437–440.

(8) Kanno, R.; Hata, T.; Kawamoto, Y.; Irie, M. Synthesis of a New Lithium Ionic Conductor, Thio-LISICON-Lithium Germanium Sulfide System. *Solid State Ionics* **2000**, *130*, 97–104.

(9) Kamaya, N.; Homma, K.; Yamakawa, Y.; Hirayama, M.; Kanno, R.; Yonemura, M.; Kamiyama, T.; Kato, Y.; Hama, S.; Kawamoto, K.; Mitsui, A. A Lithium Superionic Conductor. *Nat. Mater.* **2011**, *10*, 682-686.

(10) Kato, Y.; Hori, S.; Saito, T.; Suzuki, K.; Hirayama, M.; Mitsui, A.; Yonemura, M.; Iba, H.; Kanno, R. High-Power All-Solid-State Batteries Using Sulfide Superionic Conductors. *Nat. Energy* **2016**, *1*, 16030.

(11) Hayashi, A.; Noi, K.; Sakuda, A.; Tatsumisago, M. Superionic Glass-Ceramic Electrolytes for Room-Temperature Rechargeable Sodium Batteries. *Nat. Commun.* **2012**, *3*, 856.

(12) Anji Reddy, M.; Fichtner, M. Batteries Based on Fluoride Shuttle. *J. Mater. Chem.* **2011**, *21*, 17059–17062.

(13) Richards, W. D.; Miara, L. J.; Wang, Y.; Kim, J. C.; Ceder, G. Interface Stability in Solid-State Batteries. *Chem. Mater.* **2016**, *28*, 266–273.

(14) Zhu, Y.; He, X.; Mo, Y. Origin of Outstanding Stability in the Lithium Solid Electrolyte Materials: Insights from Thermodynamic Analyses Based on First-Principles Calculations. *ACS Appl. Mater. Interfaces* **2015**, *7*, 23685–23693.

(15) Zhu, Y.; He, X.; Mo, Y. First Principles Study on Electrochemical and Chemical Stability of Solid Electrolyte–Electrode Interfaces in All-Solid-State Li-Ion Batteries. *J. Materals Chem. A* **2016**, *4*, 3253–3266.

(16) Wenzel, S.; Leichtweiss, T.; Krüger, D.; Sann, J.; Janek, J. Interphase Formation on Lithium Solid Electrolytes - An in Situ Approach to Study Interfacial Reactions by Photoelectron Spectroscopy. *Solid State Ionics* **2015**, *278*, 98–105.

(17) Ohta, N.; Takada, K.; Sakaguchi, I.; Zhang, L.; Ma, R.; Fukuda, K.; Osada, M.; Sasaki, T. $LiNbO_3$-Coated $LiCoO_2$ as Cathode Material for All Solid-State Lithium Secondary Batteries. *Electrochem. commun.* **2007**, *9*, 1486–1490.

(18) Wenzel, S.; Randau, S.; Leichtweiß, T.; Weber, D. A.; Sann, J.; Zeier, W. G.; Janek, J. Direct Observation of the Interfacial Instability of the Fast Ionic Conductor $Li_{10}GeP_2S_{12}$ at the Lithium Metal Anode. *Chem. Mater.* **2016**, *28*, 2400–2407.

(19) Koerver, R.; Walther, F.; Aygün, I.; Sann, J.; Dietrich, C.; Zeier, W.; Janek, J. Redox-Active Cathode Interphases in Solid-State Batteries. *J. Mater. Chem. A* **2017**, *5*, 22750–22760.

(20) Wang, S.; Xu, H.; Li, W.; Dolocan, A.; Manthiram, A. Interfacial Chemistry in Solid-State Batteries: Formation of Interphase and Its Consequences. *J. Am. Chem. Soc.* **2018**, *140*, 250–257.

(21) Wenzel, S.; Sedlmaier, S. J.; Dietrich, C.; Zeier, W. G.; Janek, J. Interfacial Reactivity and Interphase Growth of Argyrodite Solid Electrolytes at Lithium Metal Electrodes. *Solid State Ionics* **2018**, *318*, 102–112.

(22) Verma, P.; Maire, P.; Novák, P. A Review of the Features and Analyses of the Solid Electrolyte Interphase in Li-Ion Batteries. *Electrochim. Acta* **2010**, *55*, 6332–6341.

(23) Veith, G. M.; Doucet, M.; Baldwin, J. K.; Sacci, R. L.; Fears, T. M.; Wang, Y.; Browning, J. F. Direct Determination of Solid-Electrolyte Interphase Thickness and Composition as a Function of State of Charge on a Silicon Anode. *J. Phys. Chem. C* **2015**, *119*, 20339–20349.

(24) Peled, E.; Golodnitsky, D.; Ardel, G. Advanced Model for Solid Electrolyte Interphase Electrodes in Liquid and Polymer Electrolytes. *J. Electrochem. Soc.* **1997**, *144*, L208–L210.

(25) Visbal, H.; Aihara, Y.; Ito, S.; Watanabe, T.; Park, Y.; Doo, S. The Effect of Diamond-like Carbon Coating on $LiNi_{0.8}Co_{0.15}Al_{0.05}O_2$ particles for All Solid-State Lithium-Ion Batteries Based on Li2S-P2S5glass-Ceramics. *J. Power Sources* **2016**, *314*, 85–92.

(26) Woo, J. H.; Trevey, J. E.; Cavanagh, A. S.; Choi, Y. S.; Kim, S. C.; George, S. M.; Oh, K. H.; Lee, S.-H. Nanoscale Interface Modification of $LiCoO_2$ by Al_2O_3 Atomic Layer Deposition for Solid-State Li Batteries. *J. Electrochem. Soc.* **2012**, *159*, A1120–A1124.

(27) Sang, L.; Bassett, K. L.; Castro, F. C.; Young, M. J.; Chen, L.; Haasch, R. T.; Elam, J. W.; Dravid, V. P.; Nuzzo, R. G.; Gewirth, A. A. Understanding the Effect of Interlayers at the Thiophosphate Solid Electrolyte/Lithium Interface for All-Solid-State Li Batteries. *Chem. Mater.* **2018**, *30*, 8747–8756.

(28) Choudhury, N. S.; Patterson, J. W. Steady-State Chemical Potential Profile in Solid Electrolytes. *J. Electrochem. Soc.* **1970**, *117*, 1384–1388.

(29) Choudhury, N. S.; Patterson, J. W. Performance Characteristics of Solid Electrolytes under Steady-State Conditions. *J. Electrochem. Soc.* **1971**, *118*, 1398–1403.

(30) Mizusaki, J.; Fueki, K.; Mukaibo, T. An Investigation of the Hebb-Wagner's d-c Polarization Technique I. Steady-State Chemical Potential Profiles in Solid Electrolytes.Pdf. *Bull. Chem. Soc. Jpn.* **1975**, *48*, 428–431.

(31) Rosenkranz, C.; Janek, J. Determination of Local Potentials in Mixed Conductors-Two Examples. *Solid State Ionics* **1995**, *82*, 95–106.

(32) Mineshige, A.; Taji, T.; Muroi, Y.; Kobune, M.; Fujii, S.; Nishi, N.; Inaba, M.; Ogumi, Z. Oxygen Chemical Potential Variation in Ceria-Based Solid Oxide Fuel Cells Determined by Raman Spectroscopy. *Solid State Ionics* **2000**, *135*, 481–485.

(33) Okuyama, Y.; Okuyama, K.; Mizutani, Y.; Sakai, T.; Lee, Y. S.; Matsumoto, H. Proton Transport Properties of $La_{0.9}Sr_{0.1}Yb_{0.8}In_{0.2}O_{3-d}$ and Its Application to Proton Ceramic Fuel Cell. *Int. J. Hydrogen Energy* **2014**, *39*, 20829–20836.

(34) Nakamura, T.; Mizunuma, S.; Kimura, Y.; Mikami, Y.; Yamauchi, K.; Kuroha, T.; Taniguchi, N.; Tsuji, Y.; Okuyama, Y.; Amezawa, K. Energy Efficiency of Ionic Transport through Proton Conducting Ceramic Electrolytes for Energy Conversion Applications. *J. Mater. Chem. A* **2018**, *6*, 15771–15780.

(35) Baumann, F. S.; Fleig, J.; Habermeier, H. U.; Maier, J. Impedance Spectroscopic Study on Well-Defined (La,Sr)(Co,Fe)O_{3-d} model Electrodes. *Solid State Ionics* **2006**, *177*, 1071–1081.

(36) Baumann, F. S.; Maier, J.; Fleig, J. The Polarization Resistance of Mixed Conducting SOFC Cathodes: A Comparative Study Using Thin Film Model Electrodes. *Solid State Ionics* **2008**, *179*, 1198–1204.

(37) Kawada, T.; Suzuki, J.; Sase, M.; Kaimai, A.; Yashiro, K.; Nigara, Y.; Mizusaki, J.; Kawamura, K.; Yugami, H. Determination of Oxygen Vacancy Concentration in a Thin Film of $La_{0.6}Sr_{0.4}CoO_{3-d}$ by an Electrochemical Method. *J. Electrochem. Soc.* **2002**, *149*, E252–E259.

(38) Nakamura, T.; Oike, R.; Kimura, Y.; Tamenori, Y.; Kawada, T.; Amezawa, K. Operando Soft X-Ray Absorption Spectroscopic Study on a Solid Oxide Fuel

Cell Cathode during Electrochemical Oxygen Reduction. *ChemSusChem* **2017**, *10*, 2008–2014.

(39) Masuda, H.; Ishida, N.; Ogata, Y.; Ito, D.; Fujita, D. Internal Potential Mapping of Charged Solid-State-Lithium Ion Batteries Using in Situ Kelvin Probe Force Microscopy. *Nanoscale* **2017**, *9*, 893–898.

(40) Yamamoto, K.; Iriyama, Y.; Asaka, T.; Hirayama, T.; Fujita, H.; Fisher, C. A. J.; Nonaka, K.; Sugita, Y.; Ogumi, Z. Dynamic Visualization of the Electric Potential in an All-Solid-State Rechargeable Lithium Battery. *Angew. Chemie - Int. Ed.* **2010**, *49*, 4414–4417.

(41) de Klerk, N. J. J.; Wagemaker, M. Space-Charge Layers in All-Solid-State Batteries; Important or Negligible? *ACS Appl. Energy Mater.* **2018**, *1*, 5609–5618.

(42) Braun, S.; Yada, C.; Latz, A. Thermodynamically Consistent Model for Space-Charge-Layer Formation in a Solid Electrolyte. *J. Phys. Chem. C* **2015**, *119*, 22281–22288.

(43) Park, J.-H.; Blumenthal, R. N. Electronic Transport in 8 Mole Percent Y_2O_3-ZrO_2. *J. Electrochem. Soc.* **1989**, *136*, 2867–2876.

(44) Wang, S.; Kobayashi, T.; Dokiya, M.; Hashimoto, T. Electrical and Ionic Conductivity of Gd-Doped Ceria. *J. Electrochem. Soc.* **2000**, *147*, 3606–3609.

(45) Maier, J. Thermodynamics of Electrochemical Lithium Storage. *Angew. Chemie - Int. Ed.* **2013**, *52*, 4998–5026.

(46) Kwon, T.; Lee, T.; Yoo, H. Partial Electronic Conductivity and Electrolytic Domain of Bilayer Electrolyte $Zr_{0.84}Y_{0.16}O_{1.92}$/$Ce_{0.9}Gd_{0.1}O_{1.95}$. *Solid State Ionics* **2011**, *195*, 25–35.

(47) Wang, Z.; Huang, X.; Lv, Z.; Zhang, Y.; Wei, B.; Zhu, X.; Wang, Z.; Liu, Z. Preparation and Performance of Solid Oxide Fuel Cells with YSZ / SDC Bilayer Electrolyte. *Ceram. Int.* **2015**, *41*, 4410–4415.

(48) Wachsman, E. D.; Lee, K. T. Lowering the Temperature of Solid Oxide Fuel Cells. *Science* **2011**, *334*, 935–939.

(49) Wachsman, E. D.; Jayaweera, P.; Jiang, N.; Lowe, D. M.; Pound, B. G. Stable High Conductivily Ceria / Bismuth Oxide Bilayered Elecfrolytes. *J. Electrochem. Soc.* **1997**, *144*, 233–236.

(50) Joh, D. W.; Park, J. H.; Kim, D.; Wachsman, E. D.; Lee, K. T. Functionally Graded Bismuth Oxide/Zirconia Bilayer Electrolytes for High-Performance Intermediate-Temperature Solid Oxide Fuel Cells (IT-SOFCs). *ACS Appl. Mater. Interfaces* **2017**, *9*, 8443–8449.

(51) Takada, K.; Ohta, N.; Zhang, L.; Fukuda, K.; Sakaguchi, I.; Ma, R.; Osada, M.; Sasaki, T. Interfacial Modification for High-Power Solid-State Lithium Batteries. *Solid State Ionics* **2008**, *179*, 1333–1337.

(52) Haruyama, J.; Sodeyama, K.; Han, L.; Takada, K.; Tateyama, Y. Space−Charge Layer Effect at Interface between Oxide Cathode and Sulfide Electrolyte in All-Solid-State Lithium-Ion Battery. *Chem. Mater.* **2014**, *26*, 4248–4255.

(53) Yada, C.; Ohmori, A.; Ide, K.; Yamasaki, H.; Kato, T.; Saito, T.; Sagane, F.; Iriyama, Y. Dielectric Modification of 5V-Class Cathodes for High-Voltage All-Solid-State Lithium Batteries. *Adv. Energy Mater.* **2014**, *4*, 1301416.

TOC graphic

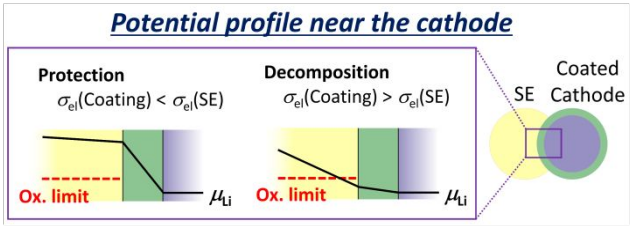
Potential profile near the cathode
Protection
σ_{el}(Coating) < σ_{el}(SE)
Decomposition
σ_{el}(Coating) > σ_{el}(SE)
Ox. limit
μ_{Li}
Ox. limit
μ_{Li}
SE
Coated
Cathode